

Real-Space, Real-Time Approach to Quantum-Electrodynamical Time-Dependent Density Functional Theory

Justin Malave,¹ Alexander Ahrens,¹ Daniel Pitagora,¹ Cody Covington,² and Kálmán Varga^{1,*}

¹*Department of Physics and Astronomy, Vanderbilt University, Nashville, Tennessee, 37235, USA*

²*Department of Chemistry, Austin Peay State University, Clarksville, USA*

The Quantum-Electrodynamical Time-Dependent Density Functional Theory (QED-TDDFT) equations are solved by time propagating the wave function on a tensor product of a Fock-space and real-space grid. Applications for molecules in cavities show the accuracy of the approach. Examples include the coupling strength and light frequency dependence of the energies, wave functions, optical absorption spectra, and Rabi splitting magnitudes in cavities, as well as a description of high harmonic generation in cavities.

I. INTRODUCTION

The possibility of altering physical and chemical properties by coupling matter to light has attracted intense experimental [1–12] and theoretical interest [13–27, 27–41, 41–59]. There are several excellent review articles highlighting the present state of the art of experimental and theoretical approaches related to light-matter interaction in cavities. These include reviews about the properties of hybrid light-matter states [60, 61], ab initio calculations [26, 62] and molecular polaritonics [63–65].

The theoretical and computational description of the coupled light matter system is challenging because the already difficult quantum many-body problem of electrons and nuclei is aggravated with the addition of the photon degrees of freedom. A plethora of approaches going beyond the simple two-level atom model [66] has been proposed in the last few years. Most of these approaches are based on successful many-body quantum methods adapted to include photon interactions. The use of the Pauli-Fierz (PF) non-relativistic quantum electrodynamics Hamiltonian is found to be the most useful framework [26, 30, 43, 51, 67] for practical calculations. The PF Hamiltonian is a sum of electronic and photonic Hamiltonians and a cross term describing the electron-photon interaction. Due to this cross term, one has to use a coupled electron-photon wave function,

$$\sum_{\vec{n}} \Phi_{\vec{n}}(\mathbf{x}) \chi_{\vec{n}} \quad (1.1)$$

where $\mathbf{x} = (\mathbf{r}_1, \mathbf{r}_2, \dots, \mathbf{R}_1, \mathbf{R}_2, \dots)$ are the spatial coordinates of the electrons and nuclei, and $\vec{n} = (n_1, n_2, \dots, N_p)$ are the quantum numbers of the photon modes. The occupation number basis, $\chi_{\vec{n}} = |n_1, n_2, \dots, N_p\rangle$, is used to represent the bosonic Fock-space of photon modes (see Appendix A for a more detailed definition).

Wave function based approaches [39, 68–71] typically use coupled electron-photon wave functions and the product form significantly increases the dimensionality. In

Refs. [37, 39, 70, 71] the coupled cluster (CC) approach is used by defining a reference wave function as a direct product of a Slater determinant of Hartree-Fock states and a zero-photon photon number state. The exponentiated cluster operator acting upon this product state defines the ground state QED-CC wave function. Systematic improvability is the greatest benefit of this approach. The stochastic variational method [68, 69] (QED-SVM) also uses a product of matter and photonic wave functions but in this case, the matter part is described by explicitly correlated Gaussian basis states [72]. The parameters of the variational ansatz are optimized by a stochastic selection process leading to highly accurate energies and wave functions. Both the QED-CC and QED-SVM approaches are limited to small atoms and molecules.

A pioneering approach to describe the interaction of light and matter in cavities is the quantum electrodynamical density functional theory (QEDFT) [40, 42, 45, 46, 73–75]. The QEDFT is an exact reformulation of the PF Hamiltonian based many-body wave theory. In practical applications of QEDFT one has to develop good approximations of the fields and currents so that the auxiliary non-interacting system generates the same physical quantities as the interacting system. To facilitate this need, the development of polaritonic exchange-correlation functionals is a focus of intense research interest [45, 76–78]. In QEDFT the spatial and photon wave functions are factorized allowing the separation of the electronic and photonic components. One then has to solve coupled equations for the matter and photon parts. The dimensionality limits the product basis approaches to a few photon modes, while the QEDFT can be applied to hundreds of thousands of photon modes [31]. More details and applications of the QEDFT method and its time-dependent version can be found in Refs. [25, 26, 28, 31, 49].

In this paper, we present a QED-DFT (and QED-TDDFT) approach using a coupled electron-photon wave function like that shown in Eq. (1.1). The wave function will be defined on a tensor product (TP) of a spatial grid and Fock state representation. To distinguish this approach from the aforementioned QEDFT approach, we will call the present approach QED-DFT-TP and QED-TDDFT-TP. The QED-DFT-TP is a particular realiza-

*Electronic address: kalman.varga@vanderbilt.edu

tion of the QEDFT theory using a different ansatz – a coupled electron-photon wave function.

The tensor product form increases the dimensionality; however, it preserves the quantized photon states. In this way, we have direct access to non-classical observables of the photon field e.g., the photon-number, the purity, or the Mandel Q number [79]. The coupled electron-photon wave function provides a more complex description of the light-matter interaction by calculating the spatial wave function in each photon sector.

Each orbital of the molecule is coupled with different Fock basis states (photon states) describing the quantized light. The light-matter coupling part of the Hamiltonian will describe the interaction between the orbital components in different photons states. The Fock states are orthogonal, preserving and even increasing the sparsity of the real-space based DFT Hamiltonian. This sparsity allows the use of the efficient iterative diagonalization approaches traditionally used in real-space DFT approaches.

As the coupling part and the product ansatz are simple, the present approach can be easily implemented in any real-space approaches. Plane-wave or orbital-based DFT methods can see similarly simple adaptation.

The approach will be tested using time-dependent and time-independent problems and our results will be compared to QED-SVM, QED-CC, and QEDFT calculations. One expects that the approach can be used everywhere where regular DFT and TDDFT have been useful, from bond length and density distribution calculations, to descriptions of high harmonic generation and optical absorption.

II. FORMALISM

A. Hamiltonian

We assume that the system is nonrelativistic and the coupling to the light can be described by the dipole approximation. The Pauli-Fierz non-relativistic QED Hamiltonian provides a consistent quantum description at this level [26, 30, 43, 51, 67]. The dipole approximation assumes that the spatial variation of the electric field is negligible across the size of the system – physically valid if the system size is much smaller than the wavelength of the light. The PF Hamiltonian in the Coulomb gauge is $H = H_e + H_{ep}$ where H_e is the electronic Hamiltonian and

$$\begin{aligned} H_{ep} &= \sum_{\alpha=1}^{N_p} \frac{1}{2} \left[p_{\alpha}^2 + \omega_{\alpha}^2 \left(q_{\alpha} - \frac{\boldsymbol{\lambda}_{\alpha}}{\omega_{\alpha}} \mathbf{D} \right)^2 \right] \\ &= \sum_{\alpha=1}^{N_p} \left[\omega_{\alpha} \left(\hat{a}_{\alpha}^+ \hat{a}_{\alpha} + \frac{1}{2} \right) - \omega_{\alpha} q_{\alpha} \boldsymbol{\lambda}_{\alpha} \mathbf{D} + \frac{1}{2} (\boldsymbol{\lambda}_{\alpha} \mathbf{D})^2 \right], \end{aligned} \quad (2.1)$$

(atomic units are used in this work). In Eq. (2.2) \mathbf{D} is the dipole operator, the photon fields are described

by quantized oscillators, and $q_{\alpha} = \frac{1}{\sqrt{2\omega_{\alpha}}} (\hat{a}_{\alpha}^+ + \hat{a}_{\alpha})$ is the displacement field. Here \hat{a} and \hat{a}^+ are, respectively, the lowering and raising operators of the quantized harmonic oscillator. This Hamiltonian describes N_p photon modes with photon frequency ω_{α} and coupling $\boldsymbol{\lambda}_{\alpha}$. The coupling term is written as [73] $\boldsymbol{\lambda}_{\alpha} = 1/\sqrt{\epsilon_0} \mathbf{u}_{\alpha}(\mathbf{r}_0)$, where $\mathbf{u}_{\alpha}(\mathbf{r})$ is the cavity mode function and \mathbf{r}_0 is the center of the cavity where the molecule is placed. The first term in Eq. (2.2) is the Hamiltonian of the photon modes, the second term couples the photons to the dipole, and the last term is the dipole self-interaction,

$$H_d = \frac{1}{2} \sum_{\alpha=1}^{N_p} (\boldsymbol{\lambda}_{\alpha} \mathbf{D})^2.$$

For the electronic Hamiltonian we adapt the Kohn-Sham (KS) TDDFT [80] description,

$$H_e = -\frac{\hbar^2}{2m} \nabla^2 + V_{KS}(\mathbf{r}), \quad (2.2)$$

with

$$V_{KS}(\mathbf{r}) = V_H[\rho](\mathbf{r}) + V_{XC}[\rho](\mathbf{r}) + V_{\text{ion}}(\mathbf{r}). \quad (2.3)$$

Here, ρ is the electron density, V_H is the Hartree potential, and V_{XC} is the exchange-correlation potential (Local density approximation (LDA) is used), and V_{ion} is the external potential due to the ions. The potential of the ions can be represented by employing the norm-conserving pseudopotentials of the form given by Troullier and Martins [81]. We assume that the nuclei are fixed in their positions.

One should emphasize at this point that the proper way of introducing the Hamiltonian would be to use mapping theorems following the steps of Ref. [27, 73, 76]. See also Ref. [77] for recent developments. Our approach can be thought to be using the conventional velocity gauge TDDFT Hamiltonian as a starting point

$$H_V = \frac{1}{2} \left(-i\hbar \nabla - \frac{e}{c} \mathbf{A} \right)^2 + V_{KS}(\mathbf{r}). \quad (2.4)$$

Then we replace the classical vector potential with the quantized vector potential of the cavity:

$$\hat{\mathbf{A}}(\mathbf{r}) = \sum_{\alpha} \left(\frac{\hbar}{2\epsilon_0 \omega_{\alpha}} \right)^{1/2} [\hat{a}_{\alpha} \mathbf{u}_{\alpha}(\mathbf{r}) + \hat{a}_{\alpha}^+ \mathbf{u}_{\alpha}^*(\mathbf{r})]. \quad (2.5)$$

In the dipole approximation, placing the molecule in the middle of the cavity at \mathbf{r}_0 one has

$$\hat{\mathbf{A}}(\mathbf{r}_0) = \sum_{\alpha} \boldsymbol{\lambda}_{\alpha} \hat{a}_{\alpha}, \quad (2.6)$$

and

$$H_V = \frac{1}{2} \left(-i\hbar \nabla - \frac{e}{c} \hat{\mathbf{A}}(\mathbf{r}_0) \right)^2 + V_{KS}(\mathbf{r}). \quad (2.7)$$

One can use a unitary transformation to transform the Hamiltonian into length gauge [67, 82]

$$H_L = U^\dagger H_V U, \quad (2.8)$$

with

$$U = \exp \left\{ -\frac{i}{\hbar} \hat{\mathbf{A}}(\mathbf{r}_0) \cdot \mathbf{D} \right\}. \quad (2.9)$$

After a straightforward calculation [67] one has

$$H_L = -\frac{\hbar^2}{2m} \nabla^2 + V_{KS}(\mathbf{r}) + \sum_{\alpha=1}^{N_p} \frac{1}{2} \left[p_\alpha^2 + \omega_\alpha^2 \left(q_\alpha - \frac{\lambda_\alpha}{\omega_\alpha} \mathbf{D} \right)^2 \right]. \quad (2.10)$$

Either H_V or H_L can be used in the calculations. The advantage of H_V is that one can use it with periodic boundary conditions. In either case, the Hamiltonian depends not only on the spatial coordinates, but on the photon creation and annihilation operators, as well and one has to use a tensor product of a spatial and number state basis for the orbitals. We will use $H = H_L$ in this work.

B. Basis functions

The $\omega_\alpha q_\alpha \lambda_\alpha \mathbf{D}$ term couples the electronic and photonic degrees of freedom. The orbitals of the coupled electron and photon system at the KS level can be written

$$\Phi_{mn} = \phi_{mn}(\mathbf{r}) |n\rangle, \quad (m = 1, \dots, N_{occ}), \quad (n = 0, \dots, N_F), \quad (2.11)$$

where $|n\rangle$ is the Fock space basis for the photons, N_F is the dimension of the Fock space, and N_{occ} is the number of orbitals. In the following we assume that there is one dominant photon mode – $N_p = 1$ in Eq. 2.2 – with frequency ω . Extension to $N_p > 1$ is possible, but it quickly leads to prohibitively large basis dimensions. We use a real-space representation [83–86] for the electronic part

$$\phi_{mn}(\mathbf{r}) = \phi_{mn}(x, y, z), \quad (2.12)$$

and the orbitals will be defined on a 4 dimensional (4D) product grid of the 3 dimensional real-space grid and the 1 dimensional Fock space. The 4D grid has $N_x \times N_y \times N_z \times (N_F + 1)$ grid points, where N_x, N_y, N_z are the grid points in real-space and N_F is the size of the Fock basis. The orbitals are written as

$$\Phi_m(\mathbf{r}) = \begin{pmatrix} \Phi_{m0}(x_i, y_j, z_k) \\ \Phi_{m1}(x_i, y_j, z_k) \\ \vdots \\ \Phi_{mn}(x_i, y_j, z_k) \\ \vdots \end{pmatrix}. \quad (2.13)$$

Due to the orthogonality of the Fock basis states we have

$$(\Phi_{mn} | \Phi_{m'n'}) = \langle \phi_{mn} | \phi_{m'n'} \rangle \delta_{nn'}, \quad (2.14)$$

where the round bracket stands for the integration over the real and Fock space and the angle bracket is the integration over the space part,

$$\langle \phi_{mn} | \phi_{m'n'} \rangle = \sum_{ijk} \phi_{mn}(x_i, y_j, z_k) \phi_{m'n'}(x_i, y_j, z_k). \quad (2.15)$$

Using Gram-Schmidt orthogonalization the real-space functions $\phi_{1n}, \dots, \phi_{N_{occ}n}$ are orthogonalized for each Fock state ($n = 0, \dots, N_F$). The new orthogonal set $\hat{\phi}_{1n}, \dots, \hat{\phi}_{N_{occ}n}$ is normalized

$$\sum_{n=0}^{N_F} |\hat{\phi}_{mn}|^2 = 1. \quad (2.16)$$

Now one can define the electron density as

$$\rho(\mathbf{r}) = \sum_{m=1}^{N_{occ}} c_m \sum_{n=0}^{N_F} |\hat{\phi}_{mn}(\mathbf{r})|^2, \quad (2.17)$$

where c_m is the number of electrons on the m th orbital. One can also define the density belonging to a given Fock state as

$$p_n(\mathbf{r}) = \sum_{m=1}^{N_{occ}} c_m |\hat{\phi}_{mn}(\mathbf{r})|^2, \quad (2.18)$$

and the photon occupation probability in the Fock space

$$P_n = \frac{1}{N} \int p_n(\mathbf{r}) d\mathbf{r}, \quad (2.19)$$

where N is the number of electrons.

The orbitals will be calculated by iterative minimization – conjugate gradient in the present case – in the same way as in the conventional real-space approaches. For this we need to calculate the action of the Hamiltonian on the wave function. Noting that

$$\omega \left(\hat{a}^+ \hat{a} + \frac{1}{2} \right) |n\rangle = \left(n + \frac{1}{2} \right) \omega |n\rangle, \quad (2.20)$$

and

$$\begin{aligned} q|n\rangle &= \frac{1}{\sqrt{2\omega}} (\hat{a} + \hat{a}^+) |n\rangle \\ &= \frac{1}{\sqrt{2\omega}} (|\sqrt{n}|n-1\rangle + \sqrt{n+1}|n+1\rangle), \end{aligned} \quad (2.21)$$

one has

$$H\Phi_{mn}(\mathbf{r}) = -\frac{1}{2}\nabla^2\Phi_{mn}(\mathbf{r}) + \left(V_{KS}(\mathbf{r}) + \mu(\boldsymbol{\lambda}\mathbf{r}) + \omega\left(n + \frac{1}{2}\right) \right) \Phi_{mn}(\mathbf{r}) - \sqrt{\frac{\omega}{2}}(\boldsymbol{\lambda}\mathbf{r}) \left(\sqrt{n}\Phi_{m,n-1}(\mathbf{r}) + \sqrt{n+1}\Phi_{m,n+1}(\mathbf{r}) \right), \quad (2.22)$$

where

$$\mu = \int \boldsymbol{\lambda}\mathbf{r}\rho(\mathbf{r})d\mathbf{r}. \quad (2.23)$$

In the first part of this equation, the Hamiltonian acts on ϕ_{mn} in each Fock space in the same way as in conventional real-space approaches. The kinetic energy operator is represented by nine-point finite differencing, and the nonlocal part of the pseudopotential is calculated by a summation in the pseudopotential core radius around the atomic position, leading to a very sparse Hamiltonian matrix. In the second part of the equation the photon spaces n and $n\pm 1$ are connected and the coupling Hamiltonian matrix is diagonal. This large sparse system is ideal for iterative approaches.

C. Ground state calculation

The ground state calculation is similar to the conventional DFT calculations:

1. Initialization of the orbitals. $\phi_{mn}^{(0)}$ are approximated e.g. by atomic orbitals. The components belonging to the lowest ($n = 0, 1$) Fock spaces are expected to be dominant so a weight factor is used to enhance those components, $\phi_{mn}^{(0)} \rightarrow w_n\phi_{mn}^{(0)}$. Orthogonalize the orbitals to generate the starting wave function

$$\hat{\Phi}_m^{(0)}(\mathbf{r}) = \begin{pmatrix} \hat{\Phi}_{m0}^{(0)}(\mathbf{r}) \\ \hat{\Phi}_{m1}^{(0)}(\mathbf{r}) \\ \vdots \\ \hat{\Phi}_{mn}^{(0)}(\mathbf{r}) \\ \vdots \end{pmatrix}, \quad (2.24)$$

where $\hat{\Phi}_{mn}^{(0)}(\mathbf{r}) = \hat{\phi}_{mn}^{(0)}(\mathbf{r})|n\rangle$.

2. Iterative minimization step. Use

$$\Phi_m^{(k+1)}(\mathbf{r}) = \sum_j a_j H^j \hat{\Phi}_m^{(k)}(\mathbf{r}), \quad (2.25)$$

where the a_j coefficients define the iterative procedure, e.g. steepest descent, conjugate gradient, imaginary time-propagation, etc. Eq. 2.22 is used to calculate $H\hat{\Phi}_{mn}^{(k)}$.

3. Calculate $\hat{\Phi}_m^{(k+1)}(\mathbf{r})$ by Gram-Schmidt orthogonalization $\Phi_m^{(k+1)}(\mathbf{r})$.
4. Calculate ρ and update V_{KS} .
5. $k=k+1$, go to step 2 until convergence is reached.

D. Time propagation

The ground state orbitals will be used to initialize the time propagation

$$\hat{\Phi}_m(\mathbf{r}, t = 0) = \hat{\Phi}_m(\mathbf{r}). \quad (2.26)$$

Any time propagation method typically used for TDDFT can be used here, and in this work we use Taylor time propagation [84]

$$\hat{\Phi}_m(\mathbf{r}, t+\Delta t) = e^{-iH\Delta t}\hat{\Phi}_m(\mathbf{r}, t) = \sum_{j=0}^4 \frac{(-i\Delta t)^j}{j!} H^j \hat{\Phi}_m(\mathbf{r}, t), \quad (2.27)$$

where Δt is chosen to be sufficiently small to conserve the norm of the orbitals during propagation.

III. APPLICATIONS

Atomic units are used in the calculations, and we drop the ‘‘a.u.’’ notation after every number. The coupling will be defined as $\boldsymbol{\lambda} = \lambda\mathbf{u}$ where \mathbf{u} is a unit vector, e.g. (1,0,0). λ can be related to the effective cavity volume $\lambda = 1/\sqrt{\epsilon_0 V_{eff}}$ (ϵ_0 is the permittivity of vacuum) [87]. Sub nm^3 volumes have been reached in picocavities [88, 89] corresponding to $\lambda < 0.05$, which will be the highest value that we consider in this work, except for an example for benzene in which we calculate the wave function in higher photon spaces.

A. Hydrogen molecule

In the first example, we calculate the energy of a hydrogen molecule in a cavity with fixed nuclei. Two-photon spaces, $|0\rangle$ and $|1\rangle$, are used. Higher photon spaces have negligible contribution for this coupling strength region. The results are compared to an SVM and a QED-CC calculation. As mentioned in the introduction, both the SVM and the QED-CC are very accurate wave function based approaches and are in complete agreement with each other in these calculations. Fig. 1 shows the total energy as a function of bond length (denoted as d) for $\lambda = 0.05$ ($\boldsymbol{\lambda} = (\lambda, 0, 0)$) and $\omega = 0.081$. The molecular bond lay parallel to the photon polarization vector. The parameters are chosen to make a comparison to the QED-CC calculations of Ref. [90]. The calculated QED-DFT-TP energy is shifted with respect to QED-CC and SVM energies, due to the LDA and pseudopotential approximations, but the overall trend is very similar. The

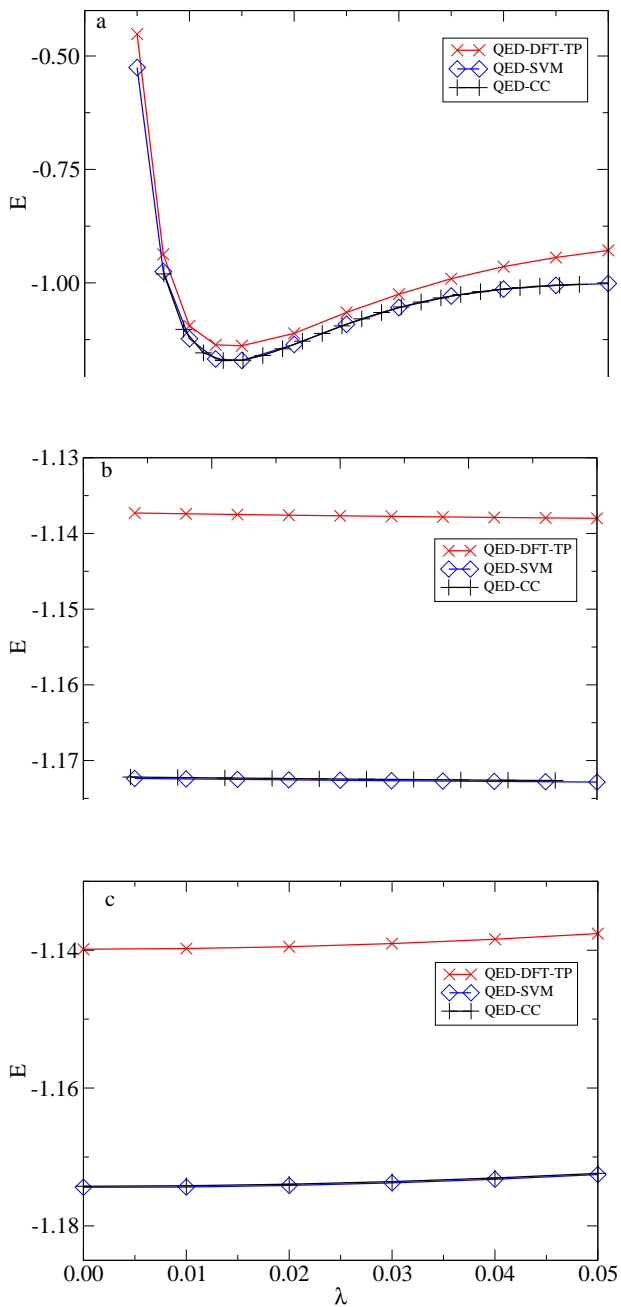


FIG. 1: Comparison of the results of the QED-DFT-TP, QED-CC and QED-SVM calculations for energy dependence on bond length (a), ω (b) and λ (c). The QED-CC results are from the calculation of Ref. [90] using cc-pVQZ basis. $\omega = 0.08$ is used for a and c, $\lambda=0.05$ is used for a and b. $N_x = N_y = N_z = 81$ and $h = 0.5$ grid spacing used in the calculations.

7

only noticeable difference is in the $2 \leq d$ region where the QED-DFT-TP curve has a larger slope. This is mainly due to the LDA approximation which performs well near the equilibrium separation, but inaccurate when the bond is stretched as it is discussed e.g. in Ref. [91].

At this coupling strength, the effect of the coupling on

the ground state is mainly an energy shift. It is more interesting to study the ω and λ dependence for a given bond length. This is shown in Figs 1 b and c. The SVM and QED-CC results are in excellent agreement, and the QED-DFT-TP results show the same behavior except for the energy shift.

Fig. 2 compares photon occupation number P_n as a function of bond length λ and ω . $N_F = 1$ is used, so $P_0 + P_1 = 1$ and only P_0 is shown in the figures. In the case of bond length, SVM and QED-DFT agree well up to $d = 1.7$. For larger distances, the two probabilities are different, probably due to the aforementioned LDA issue. The SVM and QED-DFT-TP description of the λ and ω dependence agrees well.

B. The LiH and the HF molecules

Figs. 3a and b shows the λ and ω dependence of the energy of the LiH molecule. The ω dependence calculated by QED-SVM and QED-DFT-TP are very similar. Due to the pseudopotential approach the total energies calculated by QED-DFT-TP and QED-SVM are different and the QED-SVM energies are shifted up by a constant to fit them in the same figure. We chose a larger ω ($\omega = 0.5$) for the calculation of the λ dependence to show the importance of the coupling of the $|0\rangle$ and $|1\rangle$ photon spaces. Fig. 3b shows that the energy in the $|0\rangle+|1\rangle$ case is significantly lower than in the $|0\rangle$ case for higher λ values (in the $|0\rangle$ space only the dipole self interaction is added to the Hamiltonian). The λ dependence calculated by QED-SVM and the QED-DFT-TP are in good agreement.

Figs. 3c and d shows the λ and ω dependence for a HF molecule. The ω dependence is very similar in both the QED-DFT-TP and QED-CC cases. The energy shift is due to the pseudopotential treatment of the core electrons in the QED-DFT-TP case. In this case the weight of the $|0\rangle$ space is 95% and the weight of the $|1\rangle$ space is 5% for the largest λ , so in overall the $|0\rangle$ space dominates but the $|1\rangle$ space also contributes to the energy as Fig. 3d shows.

The λ dependence only agrees in the tendency that by increasing λ the energy is increased, but the λ dependence is much larger in the QED-DFT-TP case.

C. Na₂ cluster

The next example is a Na₂ cluster with a bond length $d=5.8$. After the ground state calculation the initial wave function is excited with a delta kick (see Appendix D for details) and then time propagated. The photon coordinate $q(t)$ and the dipole moment $D_x(t)$ are shown in Fig. 4. We have calculated these quantities by the QED-TDDFT-TP and with the QEDFT approaches (see Appendix B for details). The time dependence of $q(t)$ calculated by the two methods differ greatly. This is under-

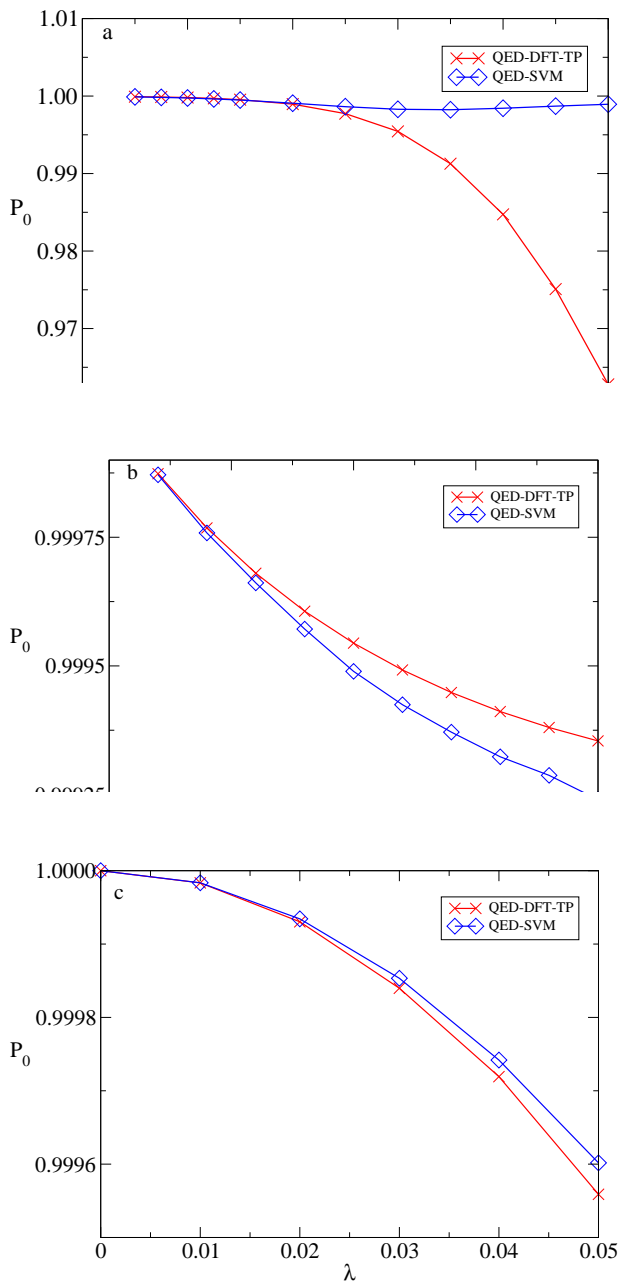


FIG. 2: Photon occupation number as a function of bond length (a), ω (b) and λ (c) . The QED-CC results are from [90]. $\omega = 0.08$ is used for a and c, $\lambda=0.05$ is used for a and b. $N_x = N_y = N_z = 81$ and $\hbar = 0.5$ used in the calculations.

standable: in the present calculation $q(t)$ is calculated by solving the time-dependent Schrödinger equation and calculating the expectation value from the time-dependent wave function comprising different photon spaces. In QEDFT, the expectation value of $q(t)$ is calculated using Eq. (B2). The dipole moments calculated by the two approaches show some similarity. But these quantities are also calculated in different ways: one is solving Eq. (B1) the other is using Eq. (2.22) in the coupled orbital and photon spaces.

What we are really interested in is the excitation spectra shown Fig. 4c. The single peak of the Na_2 spectrum when no cavity is present splits into two polariton peaks in the cavity in both QEDFT and the present calculation. The QEDFT predicts a somewhat bigger splitting but both approaches show a larger upper polariton peak. The position of the disodium peak while not in a cavity seems to be at the position of the lower polariton peak of the present calculation. This is just a coincidence: the position of the single peak shifts to higher energies with nonzero λ , and the present calculation also predicts upper and lower polaritons with respect to the single peak. We will show this next.

Fig. 4d shows the evolution of the Rabi splitting as a function of λ . Using the $|0\rangle$ space only, the dipole self-interaction changes the energy of the system and changes the position of the peak in the absorption cross section (Fig. 4d) compared to the "no cavity" case (no dipole self-interaction). By coupling the $|0\rangle$ and $|1\rangle$ photon spaces, the Rabi splitting appears in the form of two peaks: one above and one below the single peak of the $|0\rangle$ photon space case. Increasing λ the splitting is increasing as it is expected. The figure also shows the contribution from the $|0\rangle$ component in the $|0\rangle+|1\rangle$ coupled case. For small λ the $|0\rangle$ component is dominant (but there is no splitting without the coupling), but for larger λ (see Fig. 4c for $\lambda = 0.05$) the $|1\rangle$ space significantly contributes; in this case to the lower peak. Note that the width of the peaks is related to the length of the simulation time. The present model excludes physical mechanisms of line broadening. More time steps at a fixed temporal resolution result in narrower, Dirac-delta like peaks.

D. Benzene and p-nitroaniline molecules

In this section, we show how the electron density changes in different photon spaces in cavities [16]. The first example is a benzene molecule (see Fig. 5). In this case we try a larger λ to couple higher photon spaces in the wave function. The $|0\rangle$, $|1\rangle$, and $|2\rangle$ spaces are coupled and the weights of these components are 0.94, 0.056, and 0.004. The electron density of the benzene in the $|0\rangle$ photon space (Fig. 5a) is very similar to the ground state electron density. The density in the $|1\rangle$ photon space (Fig. 5b) is somewhat more compact than that in $|0\rangle$ and a density hole appears in the middle of the ring. The $|2\rangle$ density (Fig. 5c) is split perpendicular to the polarization vector $\boldsymbol{\lambda} = (\lambda, \lambda, 0)$. This split is the consequence of the symmetry breaking introduced by the $\boldsymbol{\lambda}$ dependent parts of the H_{ep} term in Eq. (2.2).

Figs 5d-i show the HOMO-2 and the HOMO orbitals. The orbitals in the $|0\rangle$ photon space remain very similar to the ground state orbitals (the slight modification due to the dipole self-interaction is not visible in the figures). The $|1\rangle$ and the $|2\rangle$ components of the HOMO-2 and HOMO orbitals (Figs. 5e, f, and 5g, i) are significantly different from the $|0\rangle$ component. In the case of

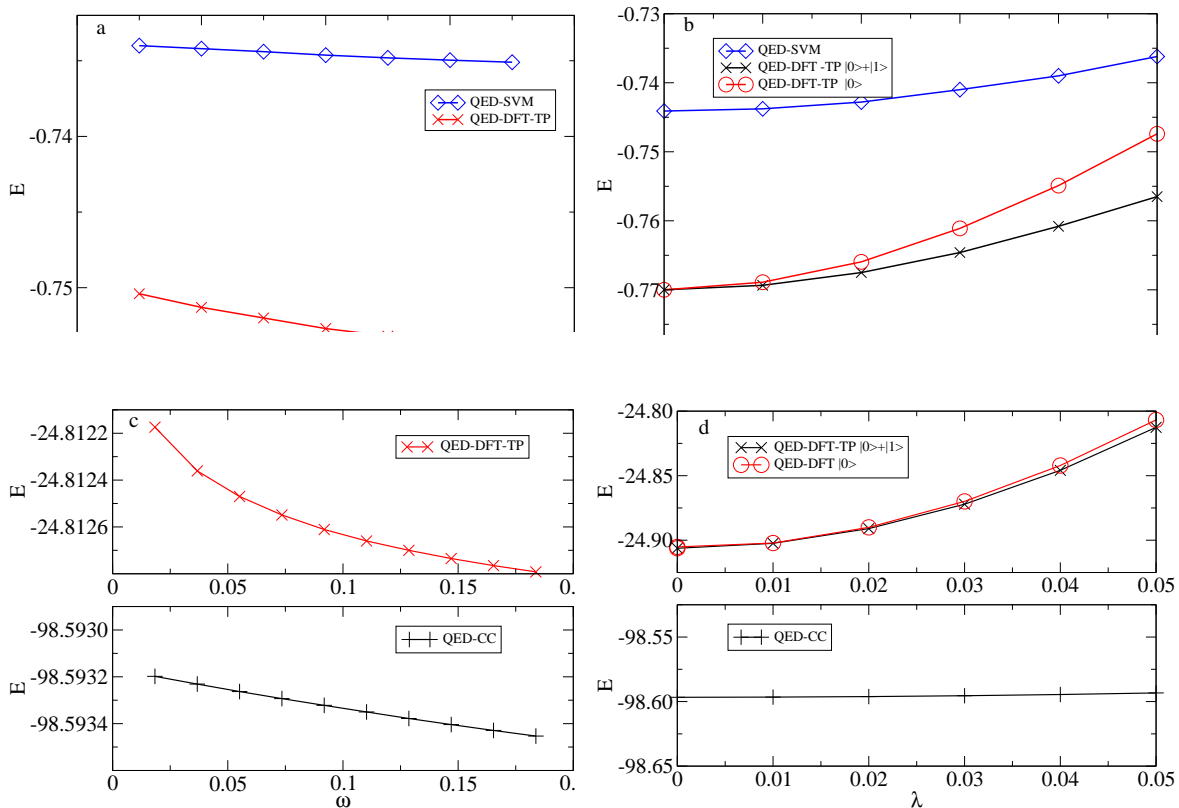


FIG. 3: Dependence of the energy of LiH and HF molecules on ω and λ . The Li-H distance is 3.015 and the H-F distance is 1.7229, $\lambda = 0.05$ was used to calculate the ω dependence for both molecules. For LiH $\omega = 0.5$, for HF $\omega = 0.0813$ was used to calculate the λ dependence. $N_x = N_y = N_z = 51$ grid points is used with $h = 0.5$ grid spacing. The QED-CC results are from [90]. In the case of the LiH molecule the QED-SVM results are shifted up by 7.3.

HOMO-2 only the charge distribution changes and the shape of the orbital components are similar, but in the case of the HOMO the lobes are also different. Other orbitals (not shown) have similar shape changes.

The next example is a p-nitroaniline molecule which was studied by QED-CC in Ref. [71] and we have adapted the parameters from that work. This is an example of a molecule with a low lying charge transfer excitation. To measure the charge transfer one can define [71]

$$\Delta q(x) = \int_{-\infty}^x dx \int_{-\infty}^{\infty} dy \int_{-\infty}^{\infty} dz \Delta \rho(x, y, z), \quad (3.1)$$

$$\Delta \rho(x, y, z) = \rho^{cavity}(x, y, z) - \rho^{nocavity}(x, y, z). \quad (3.2)$$

$\Delta q(x)$ measures the amount of charge moved in the x direction – the principle axis of the molecule. The density difference induced in the molecule by the cavity is shown in Fig. 6. The charge redistribution is very similar to what is shown in Ref. [71]. Electrons transfer from the nitro (NO_2) side to the aniline (NH_2) side. The $\Delta q(x)$ function shown in Fig. 6 is also very similar to QED-CC calculation in Ref. [71].

We have also calculated the optical absorption spectrum of the benzene molecule in a cavity by time

propagating the dipole moment after an initial delta kick perturbation. The Rabi splittings for benzene is shown in Fig. 7. The calculated splittings are 0.22 (0.33), 0.63 (0.69), 0.81 (1.02), 1.03 (1.35) for $\lambda = 0.01, 0.02, 0.03, 0.04$, respectively. The numbers in the parenthesis are from Ref. [31]. Just as in the case of the Na_2 cluster our QED-TDDFT-TP approach gives somewhat smaller Rabi splitting than the QEDFT approach, but the overall trend, a direct proportionality between the splitting and λ , is the same.

E. High harmonic generation

As a final example we present the high harmonic spectrum of the HF molecule with and without a cavity. The molecule is excited with a continuous laser pulse,

$$E(\mathbf{r}, t) = (E_x, 0, 0) \sin(\pi t / (6T_L))^2 \sin(\omega_L t) \quad (3.3)$$

and after 30 laser cycles the high harmonic spectrum is calculated using the dipole acceleration:

$$I(\omega) = \left| \int_0^T \frac{\partial^2 \mathbf{D}(t)}{\partial t^2} e^{-i\omega t} dt \right|^2. \quad (3.4)$$

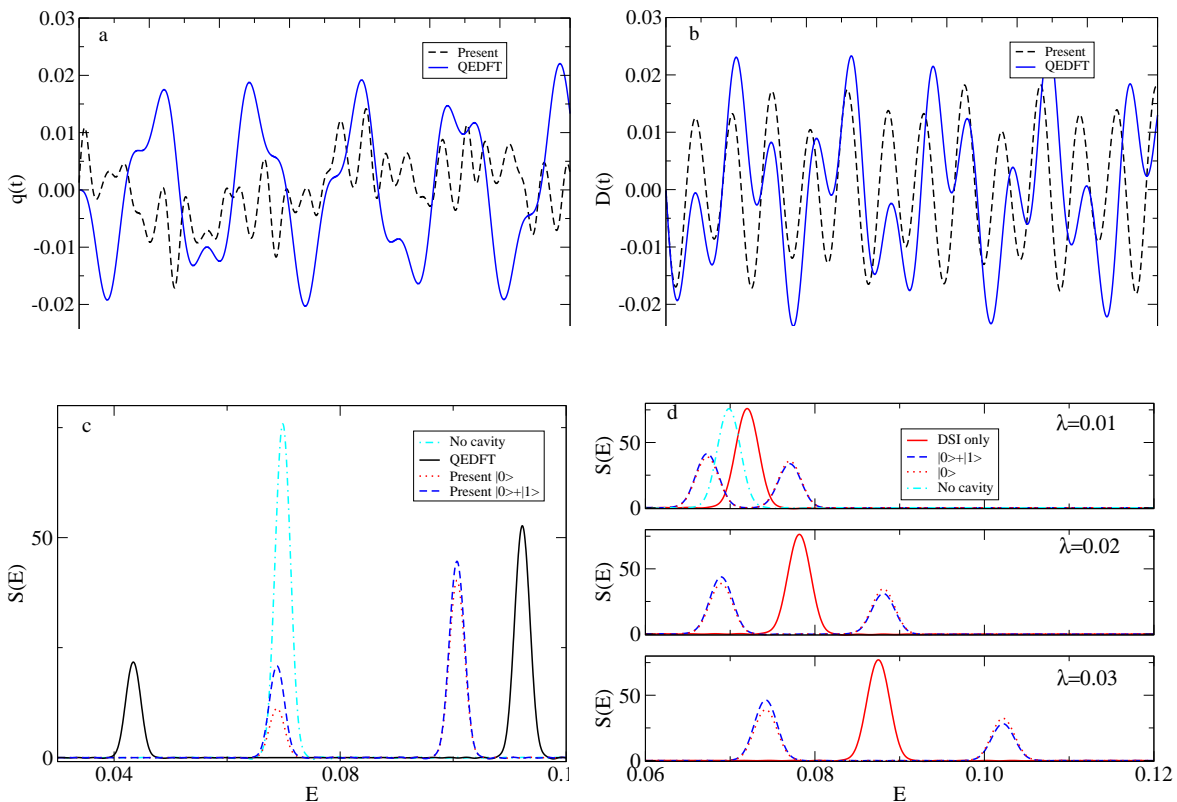


FIG. 4: QED-TDDFT-TP calculation for the Na_2 dimer. (a) Time dependence of the photon displacement coordinate. (b) Time dependence of the dipole moment. (c) Rabi splitting calculated by the QEDFT and by the present approach. $|0\rangle$ is the contribution to the absorption cross section from the 0 photon space in a calculation using $|0\rangle + |1\rangle$ space, $|0\rangle + |1\rangle$ is the total absorption cross section. $\lambda = (\lambda, 0, 0)$, $\lambda = 0.05$. (d) Dependence of the Rabi splitting on λ . DSI is the dipole self-interaction contribution. In this case the molecule is in a cavity but coupled only to the $|0\rangle$ photon space. The Na_2 dimer is oriented along the x direction and the two atoms are $d=5.8$ distance apart. $N_x = N_y = N_z = 51$, $h=0.5$, $dt=0.07$, $N_t=10000$ $d=5.8$. $\omega = 0.07$ is used in the calculations, $N_t=30000$.

Fig. 8 shows the calculated high harmonics. We are mostly interested in the first few harmonics and use a relatively small computational box to speed up the calculations. To resolve more harmonics one needs a larger box, which increases the computational cost.

If no cavity is present, the harmonic spectrum of the HF molecule oriented in the direction of the polarization of the laser consists of peaks at $n\omega_L$ (see Fig 8 for the $\omega = 0$ case). Since HF does not have inversion symmetry, both the even and odd harmonics are present. Placing the molecule in a cavity using the $|0\rangle$ photon space only, the high harmonic spectrum of the HF molecule does not change (the solid black and dotted blue lines are barely distinguishable in Fig 8).

Using the $|0\rangle + |1\rangle$ photon spaces new peaks appear in the harmonic spectrum at $\omega + n\omega_L$ positions. For example if $\omega = 0.5\omega_L$ then the new peaks are at $0.5\omega_L + n\omega_L$ (Fig. 8). These peaks have significant intensity, and the peaks are present at weaker and stronger couplings as well. If $\omega = n\omega_L$ then the new (cavity induced) peaks coincide with peaks of the laser and the spectrum remains very similar to the harmonic spectrum without a cavity. Fig. 8 also shows the contribution from the $|1\rangle$ photons spaces.

The dipole moment is the sum of the components from the $|0\rangle$ and $|1\rangle$ photon spaces, and the harmonic spectrum is a result of an interference of these terms. Fig 8 shows that in the case of $\omega = (k + 1/2)\omega_L$ ($k=0,1,2,\dots$) the $|1\rangle$ component has pronounced peaks at $\omega, \omega + \omega_L$ and $\omega + 2\omega_L$. The $|1\rangle$ photon space not only induces new peaks, but significantly contributes to their intensity as well.

IV. SUMMARY

We have developed and implemented a QED-TDDFT-TP approach that uses a direct product of a Fock space for light and a real-space grid for electrons. We have tested the approach by comparing it to accurate QED-SVM and QED-CC calculations and the results are very promising. The coupling strength and light frequency dependence of energies calculated by the present approach is very similar to the QED-SVM and QED-CC results.

One of the main advantages of the approach is that it preserves the quantized photon spaces giving direct access to non-classical photon observables. A further im-

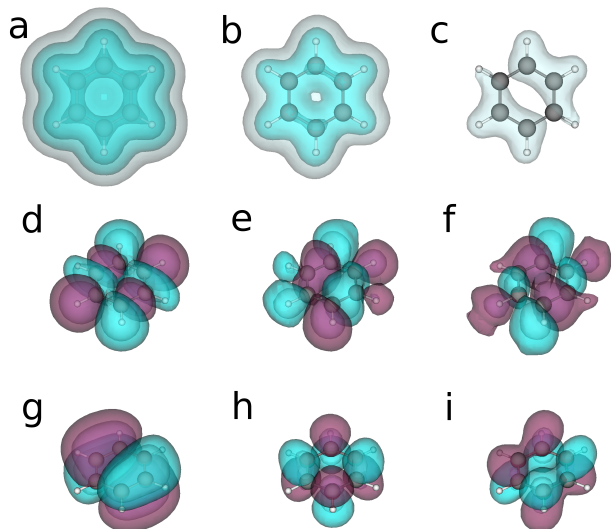


FIG. 5: Electron density ISO surfaces of benzene in the (a) $|0\rangle$, (b) $|1\rangle$, (c) $|2\rangle$ photon spaces. The three shades of the ISO surfaces have values of 0.01, 0.001, and 0.0001 HOMO-2 orbital isosurfaces of benzene in the (d) $|0\rangle$, (e) $|1\rangle$, (f) $|2\rangle$ photon spaces. HOMO orbital isosurfaces of benzene in the (g) $|0\rangle$, (h) $|1\rangle$, (i) $|2\rangle$ photon spaces. $N_x = N_y = N_z = 51$ grid points are used with $h = 0.5$ grid spacing, $\lambda = (0.1, 0.1, 0)$, $\omega = 0.5$. The darker (magenta) color shows the positive and the lighter (cyan) color shows the negative values. The two shades of the isosurfaces have values of 0.0005 and 0.0002.

portant advantage is that as the electron and the photon coordinates are separated one can assess the contribution to physical quantities from different photon spaces.

The light-matter coupling strongly modifies the molecular orbitals, and the orbitals have very different shapes in different photon spaces. This also leads to charge transfer and redistribution, and our results are similar to the QED-CC calculation [71].

We have also studied the Rabi splitting in molecules in optical cavities and the results show that the splitting is caused by the presence of light states: there is no splitting without the presence of $|0\rangle$ and $|1\rangle$ photon spaces.

The approach can also be used to study high harmonic generation in strongly coupled light-matter coupled systems. There are several recent experimental and theoretical works studying the influence of polaritons on nonlinear optical processes [92–96]. We plan to extend the present study to describe the high harmonic generation for more complex molecules. We also plan to calculate the nonlinear susceptibilities of molecules in cavities using combining the present approach with the method described in Ref. [97].

The tensor product of the real-space and Fock-space increases by the number of Fock spaces. For experimentally realizable strong coupling one needs $N_F=2$ or $N_F=3$ Fock space dimensions for a single photon frequency. This increases the cost of the calculation in time

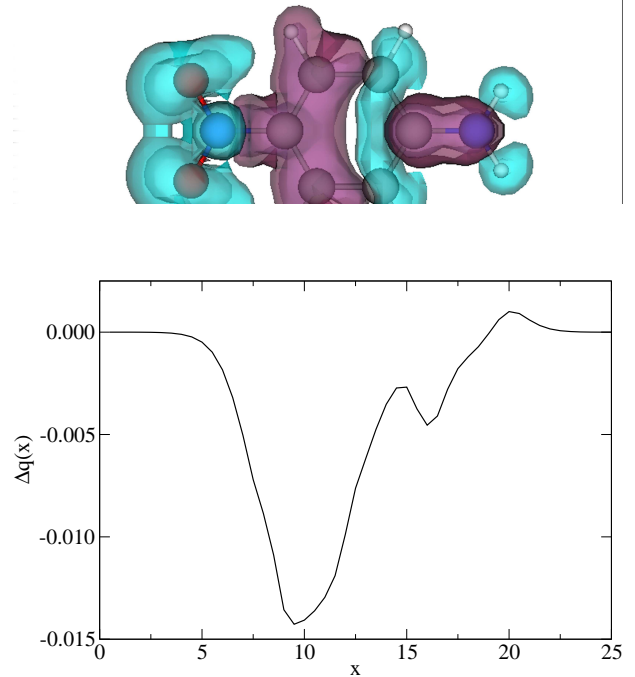


FIG. 6: (top) The cavity induced density difference between a p-nitroaniline molecule in cavity shown as isosurfaces. The two shades of the isosurfaces have values of 0.0005 and 0.0002. (bottom) Charge distribution of a p-nitroaniline molecule in cavity. $\lambda = (0.05, 0, 0)$, $\omega = 0.178$ values were used in the calculation. $N_x = N_y = N_z = 55$ grid points are used with $h = 0.5$ grid spacing. The lighter (cyan) and darker (magenta) regions represent charge depletions and accumulations, respectively.

and memory requirements by a factor of N_F . If there are more than one photon frequency is important then the calculation cost increases by $N_F^{N_p}$ where N_p is the number of relevant photon modes. For larger N_p this will be prohibitively expensive and one needs alternatives, such as the QEDFT approach, which can handle any number of photons.

The increased dimensionality is not the only complicating factor. The Hamiltonian (2.22) (except from a trivial $n\omega$ shift) acts the same way on every real-space component $\phi_{mn}(\mathbf{r}, t)$ for a given photon number. If there would be no coupling in the Hamiltonian then one would have the same set of $\phi_{mn}(\mathbf{r}, t)$, ($m = 1, \dots, N_{occ}$) orbitals in each $|n\rangle$ photon space. In the self-consistent iterative diagonalization of the nonlinear Hamiltonian, one has to carefully mix the density so that the photon components are gradually optimized. The process is very sensitive to the coupling (the off-diagonal part of the Hamiltonian), because the coupling makes the orbitals different in different photon spaces. Sudden changes in the density leads to slow damped oscillatory convergence. Future work is necessary on optimizing the self-consistent solution for this tensor product approach to have efficient calculations.

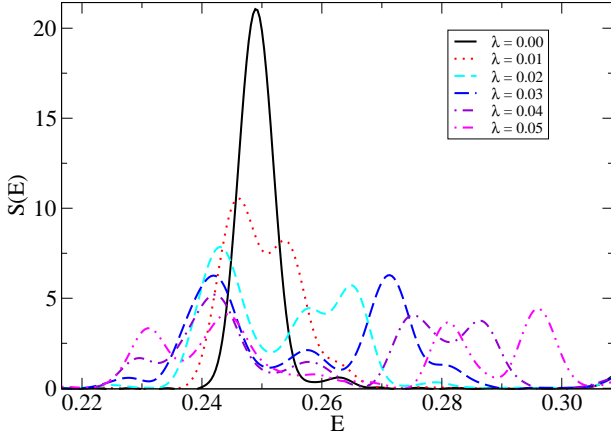


FIG. 7: Rabi splitting for benzene for different λ values. $N_x = N_y = N_z = 55$ grid points is used with $h = 0.5$ grid spacing. The time step is 0.05 and the total propagation time is 1000. $\lambda = (0, \lambda, 0)$ and $\omega = 0.25$ was used in the calculations.

The development of accurate exchange-correlation functionals are also important for future calculations. In the present work we have compared our calculations to QED-SVM and QED-CC results, and these approaches may help in developing appropriate functionals for QED-TDDFT-TP.

Acknowledgments

This work has been supported by the National Science Foundation (NSF) under Grant No. IRES 1826917. J.M., A.A. and D.P. equally contributed to this work.

Data Availability Statement

The data that support the findings of this study are available from the corresponding author upon reasonable request.

AUTHOR DECLARATIONS

Conflict of Interest

The authors have no conflict of interest to disclose.

Appendix A: Photon space

In this Appendix we give a brief overview of the properties of the Fock space and occupation number basis. The photon Hamiltonian (from Eq. (2.2))

$$H_p = \sum_{\alpha=1}^{N_p} \frac{1}{2} (p_{\alpha}^2 + \omega_{\alpha}^2 q_{\alpha}^2) = \sum_{\alpha=1}^{N_p} \omega_{\alpha} \left(\hat{a}_{\alpha}^{\dagger} \hat{a}_{\alpha} + \frac{1}{2} \right), \quad (\text{A1})$$

where

$$q_{\alpha} = \frac{1}{\sqrt{2\omega_{\alpha}}} (\hat{a}_{\alpha} + \hat{a}_{\alpha}^{\dagger}) \quad p_{\alpha} = \frac{1}{i\sqrt{2\omega_{\alpha}}} (\hat{a}_{\alpha} - \hat{a}_{\alpha}^{\dagger}). \quad (\text{A2})$$

Denoting the vacuum state as $|0\rangle$, any eigenstate of $\hat{a}_{\alpha}^{\dagger} \hat{a}_{\alpha}$ can be calculated by multiple applications of the creation operators

$$|n_{\alpha}\rangle = \frac{1}{\sqrt{n!}} (\hat{a}_{\alpha}^{\dagger})^n |0\rangle. \quad (\text{A3})$$

This is called the occupation number representation, n_{α} defines the excited state of the ω_{α} photon mode. The bosonic operators satisfy the commutation relations

$$[\hat{a}_{\alpha}, \hat{a}_{\alpha'}] = [\hat{a}_{\alpha}^{\dagger}, \hat{a}_{\alpha'}^{\dagger}] = 0, \quad [\hat{a}_{\alpha}, \hat{a}_{\alpha'}^{\dagger}] = \delta_{\alpha, \alpha'} \hat{1} \quad (\text{A4})$$

where $[a, b] = ab - ba$.

Now one can define an occupation number basis

$$\chi_{\vec{n}} = |n_1, n_2, \dots, N_p\rangle = \frac{1}{\sqrt{n_1! \dots n_{N_p}!}} (\hat{a}_1^{\dagger})^{n_1} \dots (\hat{a}_{N_p}^{\dagger})^{n_{N_p}} |0\rangle \quad (\text{A5})$$

where $n = n_1 + \dots + n_{N_p}$. In this abstract space representation the symmetry requirement for bosons is satisfied by allowing that mode i is occupied by n_i photons. For the product state in Eq. (A5) the restriction to the symmetric subspace is tacitly assumed, that is one has to symmetrize the states for identical harmonic oscillators.

Appendix B: QEDFT

In the approach of Refs. [25, 26, 28, 31, 49] two coupled equation are solved

$$i\hbar \frac{\partial}{\partial t} \varphi_i(\mathbf{r}, t) = \left(-\frac{1}{2} \nabla^2 + V_{KS}(\mathbf{r}, t) + V_P(\mathbf{r}, q, t) \right) \varphi_i(\mathbf{r}, t) \quad (\text{B1})$$

$$\left(\frac{\partial^2}{\partial t^2} + \omega_{\alpha}^2 \right) q_{\alpha}(t) = -\frac{j_{\alpha}(t)}{\omega_{\alpha}} + \omega_{\alpha} \boldsymbol{\lambda}_{\alpha} \cdot \mathbf{R}(t) \quad (\text{B2})$$

where $\mathbf{R}(t) = \int d\mathbf{r} \mathbf{r} \rho(\mathbf{r}, t)$. The photon exchange potential is

$$V_P(\mathbf{r}, q, t) = \sum_{\alpha=1}^M \left(\int d\mathbf{r}' \boldsymbol{\lambda}_{\alpha} \cdot \mathbf{r}' \rho(\mathbf{r}', t) - \omega_{\alpha} q_{\alpha}(t) \right) \boldsymbol{\lambda}_{\alpha} \mathbf{r} \quad (\text{B3})$$

The photon is propagated as

$$\left(\frac{\partial^2}{\partial t^2} + \omega_{\alpha}^2 \right) q_{\alpha}(t) = \omega_{\alpha} \boldsymbol{\lambda}_{\alpha} \mathbf{R}(t) \quad (\text{B4})$$

Appendix C: Stochastic variational approach

In this case the full Coulombic Hamiltonian is used, the Hamiltonian of an N electron system interacting with a

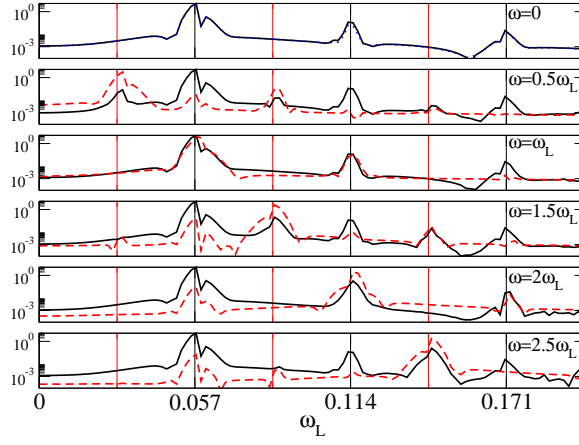


FIG. 8: High harmonics spectrum of the HF molecule (black lines). The red dashed lines show the contribution from the $|1\rangle$ photon space. The blue dotted line shows the high harmonics of the HF molecule without the cavity. The solid vertical lines show the position of $n\omega_L$, the dashed vertical lines are at $(n+1/2)\omega_L$ (where n is an integer). The axis of the molecule molecule is in the x direction, the H-F distance is 1.7229, $N_x = N_y = N_z = 51$, $h = 0.5$, $\lambda = (0.05, 0, 0)$, $\Delta t = 0.05$ and $\omega = 0.081$ is used. The laser is polarized in the x direction and the laser parameters are $\omega_L = 0.057$ (800 nm wavelength), $T_L = 2/\omega_L$ and $E_x = 0.005$.

Coulomb interaction and confined in an external potential V_c is

$$H_e = -\sum_{i=1}^N \frac{\nabla_i^2}{2m_i} + \sum_{i<j}^N \frac{q_i q_j}{|\mathbf{r}_i - \mathbf{r}_j|} + \sum_{i=1}^N V_c(\mathbf{r}_i), \quad (\text{C1})$$

where \mathbf{r}_i , q_i , and m_i are the coordinate, charge, and mass of the i th particle ($m_i = 1$ for electrons in atomic units).

Introducing the shorthand notations $\vec{r} = (\mathbf{r}_1, \dots, \mathbf{r}_N)$, the variational trial wave function is written as a linear combination of products of spatial and photon space basis functions

$$\Psi(\vec{r}) = \sum_n \sum_{k=1}^{K_n} c_k^n \psi_k^n(\vec{r}) |n\rangle. \quad (\text{C2})$$

The spatial part of the wave function is expanded into ECGs for each photon state $|n\rangle$ as

$$\psi_k^n(\vec{r}) = \mathcal{A} \left\{ e^{-\frac{1}{2} \sum_{i<j}^N \alpha_{ij}^k (\mathbf{r}_i - \mathbf{r}_j)^2 - \frac{1}{2} \sum_{i=1}^N \beta_i^k (\mathbf{r}_i - \mathbf{s}_i^k)^2} \chi_S \right\} \quad (\text{C3})$$

where \mathcal{A} is an antisymmetrizer, χ_S is the N electron spin function (coupling the spin to S), and α_{ij}^k, β_i^k and \mathbf{s}_i^k are nonlinear parameters. The basis functions are optimized as described in Ref. [68].

Appendix D: Absorption cross section

The polarizability tensor $\alpha(\omega)$ can be calculated by time propagation of the electron orbitals states. The initial state is first perturbed by a delta kick potential

$$V_{ext} = -e\mathbf{r} \cdot \mathbf{k}_i \delta(t_0), \quad (\text{D1})$$

where \mathbf{k}_i is the electric field in the i direction ($i = x, y, z$). The magnitude of the electric field should be sufficiently small to initiate a linear-response.

The polarizability tensor in frequency space is defined as the Fourier Transform of the time-dependent dipole moment

$$\alpha_{ij}(\omega) = \frac{1}{k_i} \int_0^\infty dt [D_j(t) - D_j(t_0)] e^{-i\omega t}. \quad (\text{D2})$$

The time-dependent dipole moments can be calculated from the time-dependent electronic density ($\rho(\mathbf{r}, t)$):

$$\mathbf{D}(t) = \int \mathbf{r} \cdot \rho(\mathbf{r}, t) d\mathbf{r} \quad (\text{D3})$$

The imaginary part of the dynamic polarizability tensor can be related to the oscillator strength of each transition [98]

$$\begin{aligned} \frac{1}{3} \text{Tr}[\Im m \alpha(\omega)] &= \frac{\pi}{3} \sum_{n=1}^{\infty} \sum_{\nu=1}^3 |\langle \Psi_0 | \hat{r}_\nu | \Psi_n \rangle|^2 \delta(\omega - \Omega_n) \\ &= \sum_{n=1}^{\infty} \frac{\pi}{2\Omega_n} f_n \delta(\omega - \Omega_n), \end{aligned} \quad (\text{D4})$$

where the $|\Psi_n\rangle$ is the wave function of the n -th excited state, Ω_n is the corresponding excitation energy, and f_n is the oscillator strength belonging to the transition probability for the excitation. The dynamic polarization tensor ($\alpha(\omega)$) and the transition dipole moment are now connected as ($\mathbf{D}_{n0} = \langle \Psi_0 | \hat{\mathbf{r}} | \Psi_n \rangle$).

From the imaginary part of the dynamic polarizability tensor one can extract the photo-absorption cross-section:

$$\sigma(\omega) = \frac{4\pi\omega}{3c} \text{Tr}[\Im m(\alpha(\omega))] = \frac{2\pi^2}{c} S(\omega) \quad (\text{D5})$$

where c is the speed of light and $S(\omega) = \sum_{n=1}^{\infty} f_n \delta(\omega - \Omega_n)$ is the dipole spectral function.

A damping function is added to the Fourier transform of the photo-absorption spectrum for finite propagation times. The damping function introduces an artificial de-

cah of the excited population to smooth spectrum. We use a Gaussian damping function ($e^{-\eta^2 t^2}$) and the parameter η is chosen to make the damping very small at the end of propagation.

-
- [1] J. A. Hutchison, T. Schwartz, C. Genet, E. Devaux, and T. W. Ebbesen, *Angewandte Chemie International Edition* **51**, 1592 (2012), URL <https://onlinelibrary.wiley.com/doi/pdf/10.1002/anie.201107003>, URL <https://onlinelibrary.wiley.com/doi/abs/10.1002/anie.201107003>.
- [2] R. Balili, V. Hartwell, D. Snoke, L. Pfeiffer, and K. West, *Science* **316**, 1007 (2007), ISSN 0036-8075, URL <https://science.sciencemag.org/content/316/5827/1007.full.pdf>, URL <https://science.sciencemag.org/content/316/5827/1007>.
- [3] J. Schachenmayer, C. Genes, E. Tignone, and G. Pupillo, *Phys. Rev. Lett.* **114**, 196403 (2015), URL <https://link.aps.org/doi/10.1103/PhysRevLett.114.196403>.
- [4] B. Xiang, R. F. Ribeiro, M. Du, L. Chen, Z. Yang, J. Wang, J. Yuen-Zhou, and W. Xiong, *Science* **368**, 665 (2020), ISSN 0036-8075, URL <https://science.sciencemag.org/content/368/6491/665.full.pdf>, URL <https://science.sciencemag.org/content/368/6491/665>.
- [5] A. Reserbat-Plantey, I. Epstein, I. Torre, A. T. Costa, P. A. D. Gonçalves, N. A. Mortensen, M. Polini, J. C. W. Song, N. M. R. Peres, and F. H. L. Koppens, *ACS Photonics* **8**, 85 (2021), URL <https://doi.org/10.1021/acsp Photonics.0c01224>.
- [6] D. M. Coles, N. Somaschi, P. Michetti, C. Clark, P. G. Lagoudakis, P. G. Savvidis, and D. G. Lidzey, *Nature Materials* **13**, 712 (2014), ISSN 1476-4660, URL <https://doi.org/10.1038/nmat3950>.
- [7] J. Kasprzak, M. Richard, S. Kundermann, A. Baas, P. Jeambrun, J. M. J. Keeling, F. M. Marchetti, M. H. Szymańska, R. André, J. L. Staehli, et al., *Nature* **443**, 409 (2006), ISSN 1476-4687, URL <https://doi.org/10.1038/nature05131>.
- [8] T. Schwartz, J. A. Hutchison, C. Genet, and T. W. Ebbesen, *Phys. Rev. Lett.* **106**, 196405 (2011), URL <https://link.aps.org/doi/10.1103/PhysRevLett.106.196405>.
- [9] J. D. Plumbhof, T. Stöferle, L. Mai, U. Scherf, and R. F. Mahrt, *Nature Materials* **13**, 247 (2014), ISSN 1476-4660, URL <https://doi.org/10.1038/nmat3825>.
- [10] J. A. Hutchison, A. Liscio, T. Schwartz, A. Canaguier-Durand, C. Genet, V. Palermo, P. Samorì, and T. W. Ebbesen, *Advanced Materials* **25**, 2481 (2013), URL <https://onlinelibrary.wiley.com/doi/pdf/10.1002/adma.201203682>, URL <https://onlinelibrary.wiley.com/doi/abs/10.1002/adma.201203682>.
- [11] K. Wang, M. Seidel, K. Nagarajan, T. Chervy, C. Genet, and T. Ebbesen, *Nature Communications* **12**, 1486 (2021), ISSN 2041-1723, URL <https://doi.org/10.1038/s41467-021-21739-7>.
- [12] D. N. Basov, A. Asenjo-Garcia, P. J. Schuck, X. Zhu, and A. Rubio, *Nanophotonics* **10**, 549 (2021), URL <https://doi.org/10.1515/nanoph-2020-0449>.
- [13] J. Feist and F. J. Garcia-Vidal, *Phys. Rev. Lett.* **114**, 196402 (2015), URL <https://link.aps.org/doi/10.1103/PhysRevLett.114.196402>.
- [14] O. Vendrell, *Phys. Rev. Lett.* **121**, 253001 (2018), URL <https://link.aps.org/doi/10.1103/PhysRevLett.121.253001>.
- [15] C. Schäfer and G. Johansson, *Phys. Rev. Lett.* **128**, 156402 (2022), URL <https://link.aps.org/doi/10.1103/PhysRevLett.128.156402>.
- [16] R. R. Riso, T. S. Haugland, E. Ronca, and H. Koch, *Nature Communications* **13**, 1368 (2022), ISSN 2041-1723, URL <https://doi.org/10.1038/s41467-022-29003-2>.
- [17] P. Badankó, O. Umarov, C. Fábri, G. J. Halász, and A. Vibók, *International Journal of Quantum Chemistry* **122**, e26750 (2022), URL <https://onlinelibrary.wiley.com/doi/pdf/10.1002/qua.26750>, URL <https://onlinelibrary.wiley.com/doi/abs/10.1002/qua.26750>.
- [18] G. Mazza and A. Georges, *Phys. Rev. Lett.* **122**, 017401 (2019), URL <https://link.aps.org/doi/10.1103/PhysRevLett.122.017401>.
- [19] O. Di Stefano, A. Settineri, V. Macrì, L. Garziano, R. Stassi, S. Savasta, and F. Nori, *Nature Physics* **15**, 803 (2019), ISSN 1745-2481, URL <https://doi.org/10.1038/s41567-019-0534-4>.
- [20] J. Galego, F. J. Garcia-Vidal, and J. Feist, *Phys. Rev. X* **5**, 041022 (2015), URL <https://link.aps.org/doi/10.1103/PhysRevX.5.041022>.
- [21] F. Herrera and F. C. Spano, *Phys. Rev. Lett.* **116**, 238301 (2016), URL <https://link.aps.org/doi/10.1103/PhysRevLett.116.238301>.
- [22] J. Galego, F. J. Garcia-Vidal, and J. Feist, *Nature Communications* **7**, 13841 (2016), ISSN 2041-1723, URL <https://doi.org/10.1038/ncomms13841>.
- [23] A. Shalabney, J. George, J. Hutchison, G. Pupillo, C. Genet, and T. W. Ebbesen, *Nature Communications* **6**, 5981 (2015), ISSN 2041-1723, URL <https://doi.org/10.1038/ncomms6981>.
- [24] F. Buchholz, I. Theophilou, S. E. B. Nielsen, M. Ruggenthaler, and A. Rubio, *ACS Photonics* **6**, 2694 (2019).
- [25] C. Schäfer, M. Ruggenthaler, H. Appel, and A. Rubio, *Proceedings of the National Academy of Sciences* **116**, 4883 (2019), ISSN 0027-8424, URL <https://www.pnas.org/content/116/11/4883.full.pdf>, URL <https://www.pnas.org/content/116/11/4883>.
- [26] M. Ruggenthaler, N. Tancogne-Dejean, J. Flick, H. Appel, and A. Rubio, *Nature Reviews Chemistry* **2**, 0118 (2018), ISSN 2397-3358, URL <https://doi.org/10.1038/s41570-018-0118>.
- [27] J. Flick, M. Ruggenthaler, H. Appel, and A. Rubio, *Proceedings of the National Academy of Sciences* **112**, 15285 (2015), ISSN 0027-8424, URL <https://www.pnas.org/content/112/50/15285.full.pdf>, URL <https://www.pnas.org/content/112/50/15285>.
- [28] J. Flick, M. Ruggenthaler, H. Appel, and A. Rubio, *Proceedings of the National Academy of Sciences* **114**, 3026 (2017), ISSN 0027-8424, URL <https://www.pnas.org/content/114/12/3026.full.pdf>, URL <https://www.pnas.org/content/114/12/3026>.
- [29] L. Lacombe, N. M. Hoffmann, and N. T. Maitra, *Phys. Rev. Lett.* **123**, 083201 (2019), URL

- <https://link.aps.org/doi/10.1103/PhysRevLett.123.083201>. Letters **12**, 508 (2021), pMID: 33373238, URL <https://doi.org/10.1021/acs.jpcclett.0c03436>.
- [30] A. Mandal, S. Montillo Vega, and P. Huo, The Journal of Physical Chemistry Letters **11**, 9215 (2020), pMID: 32991814.
- [31] J. Flick, D. M. Welakuh, M. Ruggenthaler, H. Appel, and A. Rubio, ACS Photonics **6**, 2757 (2019).
- [32] S. Latini, E. Ronca, U. De Giovannini, H. Hübener, and A. Rubio, Nano Letters **19**, 3473 (2019), pMID: 31046291.
- [33] J. Flick, N. Rivera, and P. Narang, Nanophotonics **7**, 1479 (2018), URL <https://doi.org/10.1515/nanoph-2018-0067>.
- [34] J. Flick and P. Narang, Phys. Rev. Lett. **121**, 113002 (2018), URL <https://link.aps.org/doi/10.1103/PhysRevLett.121.113002>.
- [35] F. J. Garcia-Vidal, C. Ciuti, and T. W. Ebbesen, Science **373** (2021), ISSN 0036-8075, <https://science.sciencemag.org/content/373/6551/eabd0336.full.pdf>, URL <https://science.sciencemag.org/content/373/6551/eabd0336>.
- [36] A. Thomas, L. Lethuillier-Karl, K. Nagaranjan, R. M. A. Vergauwe, J. George, T. Chervy, A. Shalabney, E. Devaux, C. Genet, J. Moran, et al., Science **363**, 615 (2019), ISSN 0036-8075, <https://science.sciencemag.org/content/363/6427/615.full.pdf>, URL <https://science.sciencemag.org/content/363/6427/615>.
- [37] U. Mordovina, C. Bungey, H. Appel, P. J. Knowles, A. Rubio, and F. R. Manby, Phys. Rev. Research **2**, 023262 (2020), URL <https://link.aps.org/doi/10.1103/PhysRevResearch.2.023262>.
- [38] D. S. Wang, T. Neuman, J. Flick, and P. Narang, The Journal of Chemical Physics **154**, 104109 (2021).
- [39] A. E. DePrince, The Journal of Chemical Physics **154**, 094112 (2021), URL <https://doi.org/10.1063/5.0038748>.
- [40] T. S. Haugland, C. Schäfer, E. Ronca, A. Rubio, and H. Koch, The Journal of Chemical Physics **154**, 094113 (2021), URL <https://doi.org/10.1063/5.0039256>.
- [41] N. M. Hoffmann, L. Lacombe, A. Rubio, and N. T. Maitra, The Journal of Chemical Physics **153**, 104103 (2020).
- [42] J. Flick and P. Narang, The Journal of Chemical Physics **153**, 094116 (2020), URL <https://doi.org/10.1063/5.0021033>.
- [43] A. Mandal, T. D. Krauss, and P. Huo, The Journal of Physical Chemistry B **124**, 6321 (2020), pMID: 32589846.
- [44] J. Galego, F. J. Garcia-Vidal, and J. Feist, Phys. Rev. Lett. **119**, 136001 (2017), URL <https://link.aps.org/doi/10.1103/PhysRevLett.119.136001>.
- [45] J. Flick, C. Schäfer, M. Ruggenthaler, H. Appel, and A. Rubio, ACS Photonics **5**, 992 (2018).
- [46] C. Schafer, M. Ruggenthaler, and A. Rubio, Phys. Rev. A **98**, 043801 (2018), URL <https://link.aps.org/doi/10.1103/PhysRevA.98.043801>.
- [47] D. Sidler, M. Ruggenthaler, H. Appel, and A. Rubio, The Journal of Physical Chemistry Letters **11**, 7525 (2020), pMID: 32805122, URL <https://doi.org/10.1021/acs.jpcclett.0c01556>.
- [48] I. Theophilou, M. Penz, M. Ruggenthaler, and A. Rubio, Journal of Chemical Theory and Computation **16**, 6236 (2020), pMID: 32816479, URL <https://doi.org/10.1021/acs.jctc.0c00618>.
- [49] D. Sidler, C. Schäfer, M. Ruggenthaler, and A. Rubio, The Journal of Physical Chemistry Letters **12**, 508 (2021), pMID: 33373238, URL <https://doi.org/10.1021/acs.jpcclett.0c03436>.
- [50] F. Buchholz, I. Theophilou, K. J. H. Giesbertz, M. Ruggenthaler, and A. Rubio, Journal of Chemical Theory and Computation **16**, 5601 (2020), pMID: 32692551, URL <https://doi.org/10.1021/acs.jctc.0c00469>.
- [51] I. V. Tokatly, Phys. Rev. B **98**, 235123 (2018), URL <https://link.aps.org/doi/10.1103/PhysRevB.98.235123>.
- [52] N. Rivera, J. Flick, and P. Narang, Phys. Rev. Lett. **122**, 193603 (2019), URL <https://link.aps.org/doi/10.1103/PhysRevLett.122.193603>.
- [53] T. Szidarovszky, G. J. Halász, and Á. Vibók, New Journal of Physics **22**, 053001 (2020), URL <https://doi.org/10.1088/1367-2630/ab8264>.
- [54] L. S. Cederbaum, The Journal of Physical Chemistry Letters **12**, 6056 (2021), pMID: 34165990, URL <https://doi.org/10.1021/acs.jpcclett.1c01570>.
- [55] B. Gu, and S. Mukamel, Journal of the American Chemical Society **144**, 7758 (2022), pMID: 35404593, URL <https://doi.org/10.1021/jacs.2c00921>.
- [56] F. Pavosevic and A. Rubio, The Journal of Chemical Physics **0**, null (0), URL <https://doi.org/10.1063/5.0095552>.
- [57] F. Pavošević and J. Flick, The Journal of Physical Chemistry Letters **12**, 9100 (2021), pMID: 34520211, URL <https://doi.org/10.1021/acs.jpcclett.1c02659>.
- [58] F. Pavošević, S. Hammes-Schiffer, A. Rubio, and J. Flick, Journal of the American Chemical Society **144**, 4995 (2022), pMID: 35271261, URL <https://doi.org/10.1021/jacs.1c13201>.
- [59] L. S. Cederbaum and A. I. Kuleff, Nature Communications **12**, 4083 (2021), ISSN 2041-1723, URL <https://doi.org/10.1038/s41467-021-24221-6>.
- [60] T. W. Ebbesen, Accounts of Chemical Research **49**, 2403 (2016), URL <https://doi.org/10.1021/acs.accounts.6b00295>.
- [61] C. Genet, J. Faist, and T. W. Ebbesen, Physics Today **74**, 42 (2021), URL <https://doi.org/10.1063/PT.3.4749>.
- [62] D. Sidler, M. Ruggenthaler, C. Schäfer, E. Ronca, and A. Rubio, The Journal of Chemical Physics **156**, 230901 (2022), URL <https://doi.org/10.1063/5.0094956>.
- [63] T. E. Li, B. Cui, J. E. Subotnik, and A. Nitzan, Annual Review of Physical Chemistry **73**, 43 (2022), URL <https://doi.org/10.1146/annurev-physchem-090519-042621>.
- [64] M. Sánchez-Barquilla, A. I. Fernández-Domínguez, J. Feist, and F. J. García-Vidal, ACS Photonics **9**, 1830 (2022), URL <https://doi.org/10.1021/acsp Photonics.2c00048>.
- [65] J. Fregoni, F. J. Garcia-Vidal, and J. Feist, ACS Photonics **9**, 1096 (2022), URL <https://doi.org/10.1021/acsp Photonics.1c01749>.
- [66] E. Jaynes and F. W. Cummings (1962).
- [67] V. Rokaj, D. M. Welakuh, M. Ruggenthaler, and A. Rubio, Journal of Physics B: Atomic, Molecular and Optical Physics **51**, 034005 (2018), URL <https://doi.org/10.1088/1361-6455/aa9c99>.
- [68] A. Ahrens, C. Huang, M. Beutel, C. Covington, and K. Varga, Phys. Rev. Lett. **127**, 273601 (2021), URL <https://link.aps.org/doi/10.1103/PhysRevLett.127.273601>.
- [69] M. Beutel, A. Ahrens, C. Huang, Y. Suzuki, and K. Varga, The Journal of Chemical Physics **155**, 214103

- (2021), URL <https://doi.org/10.1063/5.0066427>.
- [70] M. D. Liebenthal, N. Vu, and A. E. DePrince, *The Journal of Chemical Physics* **156**, 054105 (2022), URL <https://doi.org/10.1063/5.0078795>.
- [71] T. S. Haugland, E. Ronca, E. F. Kjønstad, A. Rubio, and H. Koch, *Phys. Rev. X* **10**, 041043 (2020), URL <https://link.aps.org/doi/10.1103/PhysRevX.10.041043>.
- [72] J. Mitroy, S. Bubin, W. Horiuchi, Y. Suzuki, L. Adamowicz, W. Cencek, K. Szalewicz, J. Komasa, D. Blume, and K. Varga, *Rev. Mod. Phys.* **85**, 693 (2013), URL <https://link.aps.org/doi/10.1103/RevModPhys.85.693>.
- [73] M. Ruggenthaler, J. Flick, C. Pellegrini, H. Appel, I. V. Tokatly, and A. Rubio, *Phys. Rev. A* **90**, 012508 (2014), URL <https://link.aps.org/doi/10.1103/PhysRevA.90.012508>.
- [74] I. V. Tokatly, *Phys. Rev. Lett.* **110**, 233001 (2013), URL <https://link.aps.org/doi/10.1103/PhysRevLett.110.233001>.
- [75] J. Yang, Q. Ou, Z. Pei, H. Wang, B. Weng, Z. Shuai, K. Mullen, and Y. Shao, *The Journal of Chemical Physics* **155**, 064107 (2021), URL <https://doi.org/10.1063/5.0057542>.
- [76] C. Pellegrini, J. Flick, I. V. Tokatly, H. Appel, and A. Rubio, *Phys. Rev. Lett.* **115**, 093001 (2015), URL <https://link.aps.org/doi/10.1103/PhysRevLett.115.093001>.
- [77] C. Schafer, F. Buchholz, M. Penz, M. Ruggenthaler, and A. Rubio, *Proceedings of the National Academy of Sciences* **118**, e2110464118 (2021), <https://www.pnas.org/doi/pdf/10.1073/pnas.2110464118>, URL <https://www.pnas.org/doi/abs/10.1073/pnas.2110464118>.
- [78] J. Flick, *Simple exchange-correlation energy functionals for strongly coupled light-matter systems based on the fluctuation-dissipation theorem* (2021), URL <https://arxiv.org/abs/2104.06980>.
- [79] L. Mandel, *Opt. Lett.* **4**, 205 (1979), URL <http://opg.optica.org/ol/abstract.cfm?URI=ol-4-7-205>.
- [80] E. Runge and E. K. U. Gross, *Phys. Rev. Lett.* **52**, 997 (1984).
- [81] N. Troullier and J. L. Martins, *Phys. Rev. B* **43**, 1993 (1991).
- [82] M. A. D. Taylor, A. Mandal, and P. Huo, *Opt. Lett.* **47**, 1446 (2022), URL <http://opg.optica.org/ol/abstract.cfm?URI=ol-47-6-1446>.
- [83] J. R. Chelikowsky, N. Troullier, and Y. Saad, *Phys. Rev. Lett.* **72**, 1240 (1994), URL <https://link.aps.org/doi/10.1103/PhysRevLett.72.1240>.
- [84] K. Yabana and G. F. Bertsch, *Phys. Rev. B* **54**, 4484 (1996), URL <https://link.aps.org/doi/10.1103/PhysRevB.54.4484>.
- [85] N. Tancogne-Dejean, M. J. T. Oliveira, X. Andrade, H. Appel, C. H. Borca, G. Le Breton, F. Buchholz, A. Castro, S. Corni, A. A. Correa, et al., *The Journal of Chemical Physics* **152**, 124119 (2020), URL <https://doi.org/10.1063/1.5142502>.
- [86] K. Varga, Z. Zhang, and S. T. Pantelides, *Phys. Rev. Lett.* **93**, 176403 (2004), URL <https://link.aps.org/doi/10.1103/PhysRevLett.93.176403>.
- [87] J. Galego, C. Climent, F. J. Garcia-Vidal, and J. Feist, *Phys. Rev. X* **9**, 021057 (2019), URL <https://link.aps.org/doi/10.1103/PhysRevX.9.021057>.
- [88] F. Benz, M. K. Schmidt, A. Dreismann, R. Chikkaraddy, Y. Zhang, A. Demetriadou, C. Carnegie, H. Ohadi, B. de Nijs, R. Esteban, et al., *Science* **354**, 726 (2016), <https://www.science.org/doi/pdf/10.1126/science.aah5243>, URL <https://www.science.org/doi/abs/10.1126/science.aah5243>.
- [89] C. Carnegie, J. Griffiths, B. de Nijs, C. Readman, R. Chikkaraddy, W. M. Deacon, Y. Zhang, I. Szabó, E. Rosta, J. Aizpurua, et al., *The Journal of Physical Chemistry Letters* **9**, 7146 (2018), URL <https://doi.org/10.1021/acs.jpcllett.8b03466>.
- [90] J. D. Mallory and A. E. D. I. au₂, *Reduced-density-matrix-based ab initio cavity quantum electrodynamics* (2022), 2204.00725.
- [91] A. D. Becke, *The Journal of Chemical Physics* **140**, 18A301 (2014), URL <https://doi.org/10.1063/1.4869598>.
- [92] A. F. Kockum, V. Macrì, L. Garziano, S. Savasta, and F. Nori, *Scientific Reports* **7**, 5313 (2017), ISSN 2045-2322, URL <https://doi.org/10.1038/s41598-017-04225-3>.
- [93] T. Chervy, J. Xu, Y. Duan, C. Wang, L. Mager, M. Frerejean, J. A. W. Münninghoff, P. Tinne-mans, J. A. Hutchison, C. Genet, et al., *Nano Letters* **16**, 7352 (2016), pMID: 27960510, URL <https://doi.org/10.1021/acs.nanolett.6b02567>.
- [94] F. Barachati, J. Simon, Y. A. Getmanenko, S. Barlow, S. R. Marder, and S. Kéna-Cohen, *ACS Photonics* **5**, 119 (2018), URL <https://doi.org/10.1021/acsphotonics.7b00305>.
- [95] B. Liu, M. Crescimanno, R. J. Twieg, and K. D. Singer, *Advanced Optical Materials* **7**, 1801682 (2019), <https://onlinelibrary.wiley.com/doi/pdf/10.1002/adom.201801682>, URL <https://onlinelibrary.wiley.com/doi/abs/10.1002/adom.201801682>.
- [96] D. M. Welakuh and P. Narang, *Tunable non-linearity and efficient harmonic generation from a strongly coupled light-matter system* (2022), URL <https://arxiv.org/abs/2203.00691>.
- [97] V. A. Goncharov and K. Varga, *The Journal of Chemical Physics* **137**, 094111 (2012), URL <https://doi.org/10.1063/1.4749793>.
- [98] C. A. Ullrich, *Time-Dependent Density-Functional Theory: Concepts and Applications* (Oxford University Press, USA, 2012).